Chemical Engineering Journal 350 (2018) 436–444

Contents lists available at ScienceDirect

Chemical Engineering Journal

journal homepage: www.elsevier.com/locate/cej

Light-responsive UiO-66-NH_2/Ag_3PO_4 MOF-nanoparticle composites for the capture and release of sulfamethoxazole

Xue-Yan Xu[a], Chun Chu[a], Huifen Fu[a], Xue-Dong Du[a], Peng Wang[a], Weiwei Zheng[b], Chong-Chen Wang[a,*]

[a] Beijing Key Laboratory of Functional Materials for Building Structure and Environment Remediation, Beijing University of Civil Engineering and Architecture, Beijing 100044, PR China
[b] Department of Chemistry, Syracuse University, Syracuse, NY 13244, United States

HIGHLIGHTS

- The MOF-nanoparticle (UiO-66-NH_2/Ag_3PO_4) composites was facilely fabricated.
- The light-responsive MOF-NP composites for SMX capture and release was reported.
- The SMX release from composites was controlled by the size of nano-Ag_3PO_4 on MOF.
- Mechanism of the light-triggered SMX release was clarified.

GRAPHICAL ABSTRACT

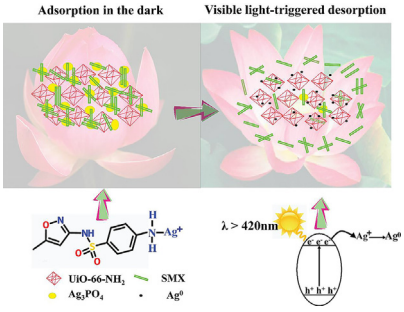

ARTICLE INFO

Keywords:
Light-response
MOF-nanoparticle composites
Desorption
UiO-66-NH_2
PPCPs
Mechanism

ABSTRACT

Light-responsive materials are attracting increasing amount of attention and have great potential in many research fields in environmental chemistry, materials science, biology, and nanotechnology. In this work, UiO-66-NH_2/Ag_3PO_4 (UAP-X) Metal-organic framework (MOF)-nanoparticle composites with remarkable adsorption performance toward sulfamethoxazole (SMX) were reported. In addition, visible light-triggered release of SMX in the UAP-X composites was reported for the first time. It is believed that the light-triggered desorption of SMX is due to the transformation from Ag^+ to Ag^0 in the light-sensitive Ag_3PO_4 nanoparticles (NPs) of the composites. The SMX release performance of UAP-X can be tuned by the size of Ag_3PO_4 NPs distributed on the UiO-66-NH_2. Specifically, the smaller crystal size of Ag_3PO_4 NPs, which can facilitate the reduction of Ag^+ to Ag^0, can be achieved with an increase in relative UiO-66-NH_2 content in the composites. In addition, the higher UiO-66-NH_2 content of the composite could provide more deposition area to minimize the aggregation of Ag_3PO_4, which could further enhance the reduction of Ag^+. The light triggered desorption provides new possibility to achieve pollution-free and low-cost recyclability of adsorbents.

1. Introduction

Pharmaceuticals and personal care products (PPCPs) are widely used and essential in daily life. However, the extensive applications and poor elimination of PPCPs by the conventional biological wastewater treatment plants lead to the contamination of surface water and even ground water [1,2]. The bioaccumulation of these pseudo persistent PPCPs in the aquatic life can exert serious threat to the environment

* Corresponding author.
E-mail addresses: chongchenwang@126.com, wangchongchen@bucea.edu.cn (C.-C. Wang).

https://doi.org/10.1016/j.cej.2018.06.005
Received 3 May 2018; Received in revised form 29 May 2018; Accepted 1 June 2018
Available online 02 June 2018
1385-8947/

and ecosystem [3,4]. Sulfamethoxazole (SMX) is a type of sulfonamide (SA) that is widely used in human and veterinary pharmaceuticals to prevent and/or treat disease such as diminishing inflammation and to promote livestock growth [5]. Considering their widespread consumption, high stability in aquatic media, and low biodegradability, SAs are considered a substantial ecotoxicological threat to aquatic flora and fauna and to human health [6].

Up to now, various methods including photodegradation [7,8], coagulation-flocculation [9], biodegradation [10], chlorination [11], advanced oxidation processes (AOPs), ozonation [12,13] and adsorption [14–19], have been adopted to eliminate PPCPs from the drinking water or wastewater. The removal of PPCPs by adsorption has been drawing significant interest as it is simple and cost effective. Metal-organic frameworks (MOFs) are particularly attractive adsorbents due to their unprecedented internal volume providing a large storage capacity [20–22], and tunable framework chemistries offering a pathway to tailor release properties [23,24]. Hill and coworkers coated an optical fiber with a stable UiO-66, in which an anticancer drug 5-fluorouracil (5-FU) was loaded using a sublimation procedure [23]. The release of 5-FU into the surrounding solution was triggered by 1050 nm light. Zhou and co-workers synthesized PCN-123 to achieve reversible alteration of CO_2 capture upon photochemical and thermal treatment [25]. The combination of the high surface areas of MOFs with nanoparticles are an emergent class of composite materials. The unique size and surface effect of nanoparticle [26,27] with desirable photo-physical behavior can lead enhanced properties of MOF-NP composites [28]. For example, Ag_3PO_4 semiconductor NPs are an active visible-light-driven photocatalyst for dye degradation and oxygen evolution from water splitting [29,30].

It should be noted that conventional adsorption is usually a spontaneous process, hence desorption generally needs chemical or energy input. Recently, stimuli-responsive materials have attracted extensive attention for their potential applications in adsorption and other processes based on molecular logic systems [31–33]. Among various stimuli including heat, pH, light, magnetic and electric fields, light is highly desired and has many advantages because of (1) finely tunable with high spatial and temporal accuracy, (2) non-invasive to the environment on demand, (3) free of transport limitations, (4) no by-product generation, and (5) abundant sunlight available [31–33]. However, light-response MOF-NP composites are less explored and MOF-Ag_3PO_4 composites have not been reported to the best of our knowledge.

In this paper, a series of UiO-66-NH_2/Ag_3PO_4 composites (UAP-X, X = 20 mg, 35 mg, 50 mg, 120 mg and 200 mg UiO-66-NH_2 in the composites) were synthesized in aqueous solution via an in-situ ion-exchange deposition/precipitation method using $AgNO_3$, $Na_2HPO_4{\cdot}12H_2O$ and UiO-66-NH_2 as precursors. By the combination of the light-sensitive Ag_3PO_4 to UiO-66-NH_2, the resulting UAP-X composites demonstrated enhanced adsorption and desorption toward SMX under dark and visible-light conditions. To the best of our knowledge, it is the first report that MOF-NP composite was utilized to conduct light-triggered desorption toward organic matters.

2. Experimental

2.1. Materials and instruments

All chemicals were used directly as received without further purification. Powder X-ray diffraction (PXRD) patterns of the samples were obtained with a Dandonghaoyuan DX-2700B diffractometer in the range of $2\theta = 5°–90°$ with Cu Kα radiation. Thermogravimetric analysis (TGA) were performed from 70 to 800 °C in an air stream at a heating rate of 10 °C/min on a DTU-3c thermal analyzer using α-Al_2O_3 as a reference. The Fourier transform infrared (FTIR) spectra were recorded from KBr pellets on a Nicolet 6700 spectrometer in the range of 4000–400 cm^{-1}. The surface area of the sample was obtained from N_2 adsorption-desorption isotherms at 77 K using the Brunauer-Emmett-Teller nitrogen absorption method (BET, BELSORP-Mini II). The morphologies of the samples were observed using a JEM 1200EX transmission electron microscopy (TEM) and JEOL JSM-6700F scanning electron microscope (SEM). X-ray photoelectron spectra (XPS) measurement was performed on a Thermo ESCALAB 250XI. An Acquity UPLC H-Class (Waters) was used to detect the concentration of the SMX in solution after adsorption-desorption experiment at 274 nm. The analytes were separated by a C18 (1.7 μm, 2.1 × 50 mm) on UPLC equipped with a TUV detector. Acidified water (0.1% formic acid, *v/v*) and methanol were used as mobile phase A and B, respectively. Gradient was programmed as the following: 0 min, 10% B; 4.0 min, 10% B; 5.5 min, 65% B, 6.0 min 10% B. The column temperature was maintained at 313 K. A 6530 Q-TOF LC/MS (Agilent Technologies) was used to detect the SMX released from the UAP-X after adsorption-desorption. The 6530 Q-TOF LC/MS was equipped with a Dual AJS electrospray ionization source (ESI). Parameters for analysis were set in both positive and negative ion modes. The optimal values of the ion source parameters were: capillary, +3500 V; drying gas temperature, 523 K; drying gas flow, 7.0 L/min; nebulizer pressure, 35 psi; shealth gas temperature, 598 K and shealth gas flow, 11.0 L/min.

2.2. Synthesis of UiO-66-NH_2/Ag_3PO_4 composites

The UiO-66-NH_2 was prepared according to a reported method by Karl Petter Lillerud and coworkers with a small modification [34]. Briefly, 0.81 g (4.5 mmol) NH_2-BDC and 1.05 g (4.5 mmol) $ZrCl_4$ were dissolved in 40.0 mL DMF. Then 17.0 mL (0.3 mmol) acetic acid was added as a modulator. After that, the suspension was transferred to a Teflon-lined stainless steel autoclave and heated at 135 °C for 24 h. After the solvothermal reaction, the autoclave was slowly cooled down to room temperature. After separation from the solution via centrifugation, white solid products were ultrasonically washed with distilled water several times, then re-collected and dried under 60 °C in an oven.

UiO-66-NH_2/Ag_3PO_4 (UAP-X) composites were prepared via an in-situ ion-exchange precipitation method [29,35,36]. Firstly, appropriate amount of as-prepared UiO-66-NH_2 was dispersed in 100.0 mL of distilled water and sonicated for 30.0 min. Then, 0.10 g $AgNO_3$ was added and sonicated for another 30.0 min. After that, 0.07 g $Na_2HPO_4{\cdot}12H_2O$ was dissolved in 10.0 mL of distilled water and added dropwise into the above solution under vigorous stirring. After stirring for 4 h, the final products were collected via filtration, washed with distilled water several times and then dried under 60 °C in an oven for further characterization. Series of UiO-66-NH_2/Ag_3PO_4 composites synthesized with 20 mg, 35 mg, 50 mg, 120 mg, 200 mg of UiO-66-NH_2 were marked as UAP-20, UAP-35, UAP-50, UAP-120, UAP-200, respectively. For comparison, pure Ag_3PO_4 particles were also prepared under the same conditions without the UiO-66-NH_2 particles.

2.3. Adsorption-desorption experiment

The adsorption-desorption activities of UAP-X toward sulfamethoxazole (SMX) were carried out at 25 °C in a 50 mL quartz reactor containing 40.0 mL 50.0 mg/L SMX aqueous solution suspended with 10.0 mg UAP-X particles. After being stirred for 60 min to reach adsorption–desorption equilibrium in the dark, the suspensions were irradiated by a 350 mW LED lamp (PCX50A, Beijing Perfect Light Technology Co., Ltd) to provide visible light with wavelength longer than 420 nm (Fig. S1 in ESI†). During the adsorption-desorption process triggered by visible light, the samples were collected at regular time intervals using a 0.22 μm syringe filter to remove the composites particles before UPLC analysis. Q-TOF LC/MS was further introduced to scan the contents of the treated samples to confirm the desorption activities of UAP-X toward SMX under visible light irradiation.

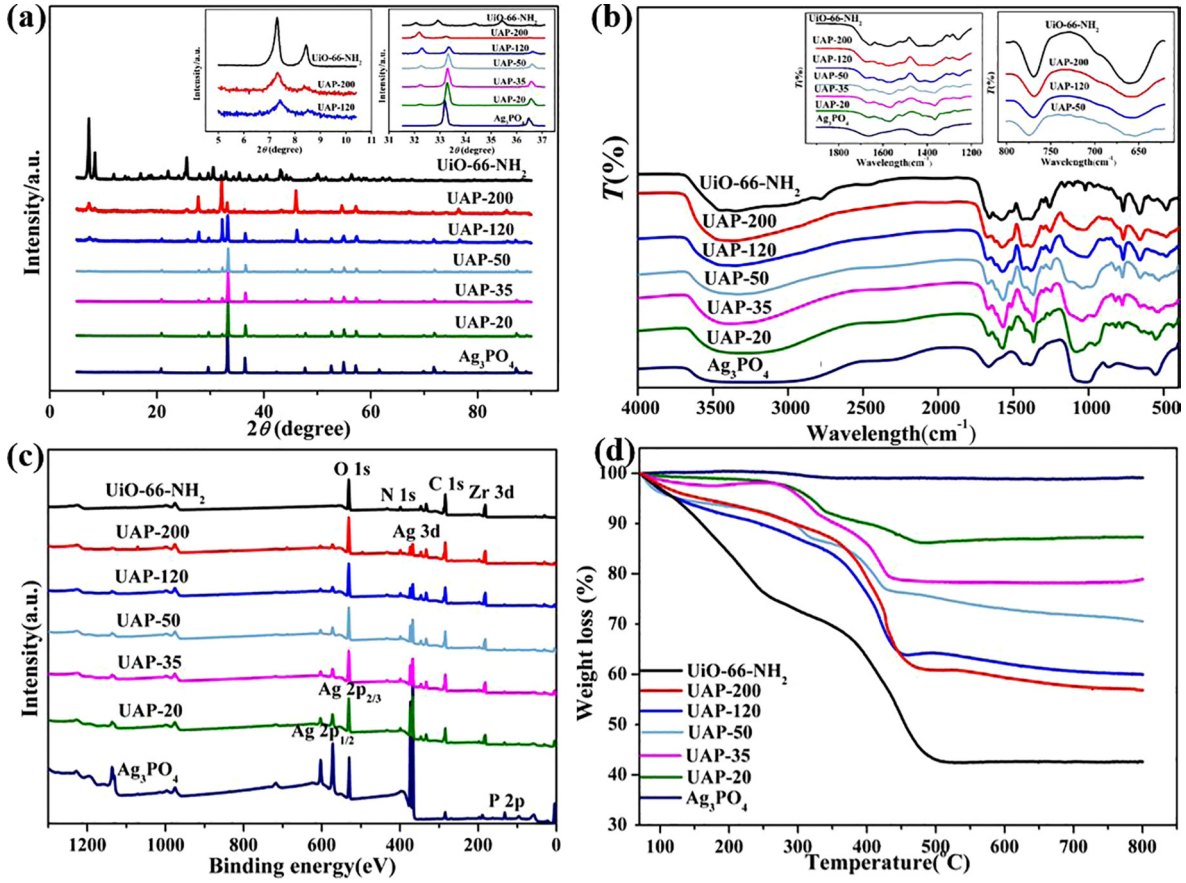

Fig. 1. (a) PXRD patterns (b) FTIR spectra (c) XPS spectra (d) TGA curves of Ag_3PO_4, UAP-X (X = 20 mg, 35 mg, 50 mg, 120 mg and 200 mg) composites and UiO-66-NH_2.

3. Results and discussion

3.1. Characterizations of UAP-X composites

The successful preparation of UAP-X composites was confirmed by PXRD, FTIR, XPS, TGA, SEM, TEM and BET analysis. The PXRD patterns of individual Ag_3PO_4, UiO-66-NH_2 and series UAP-X are illustrated in Fig. 1a. The PXRD patterns of UiO-66-NH_2 are consistent with those reported in the literatures [37,38], demonstrating pure and well crystallized UiO-66-NH_2 of the as-prepared samples. All 2θ peaks of UiO-66-NH_2 were consistent with the UiO-66 [39], indicating that the introduction of –NH_2 groups functionalized terephthalic acid does not affect the skeleton of UiO-66. The diffraction peaks of as prepared Ag_3PO_4 match perfectly with standard patterns of body-centered cubic Ag_3PO_4 crystal (JCPDS card No. 006-0505) (Fig. S2 in ESI†). The UAP-X composites exhibit almost all the characteristic PXRD peaks of UiO-66-NH_2 and Ag_3PO_4. The slight different XRD peak intensities of the samples might be resulted from the different relative content of UiO-66-NH_2 and Ag_3PO_4 and the possible preferred orientation of the crystalline UiO-66-NH_2 and Ag_3PO_4 in the composites as well. For example, the XRD patterns of UAP-120 (Fig. 1a) show the characteristic peaks of both UiO-66-NH_2 and Ag_3PO_4, indicating the introduction of UiO-66-NH_2 has no effect on the crystal structure of Ag_3PO_4. However, no obvious characteristic diffractions for Ag_3PO_4 can be observed in the UAP-200, which could be ascribed to the relatively low amount of Ag_3PO_4. The unchanged backbones of UiO-66-NH_2 and Ag_3PO_4 in series UAP-X composites were further confirmed by the similar FTIR spectra as shown in Fig. 1b. Two wide and medium adsorptions at 3507 cm^{-1} and 3384 cm^{-1} can be assigned to the aromatic amino groups in UiO-66-NH_2 [37]. The adsorption peaks between 600 and 800 cm^{-1} are contributed to Zr-O_2 as longitudinal and transverse modes [40], which was relative weak at lower UiO-66-NH_2 content (UAP-20 and UAP-35) for UAP-X composites. The intense doublet at 1421 and 1387 cm^{-1} can be assigned to the stretching modes of the carboxylic groups in NH_2-BDC ligands [41,42]. The typical P-O stretching vibrations of PO_4^{3-} can be observed at 554 and 1014 cm^{-1} [43].

The successful fabrication of UAP-X (UiO-66-NH_2/Ag_3PO_4) was further affirmed by the surface compositions and chemical state investigation via XPS analysis, as illustrated in Fig. 1c. All the binding energies obtained from the XPS analysis were corrected by referencing C1s to 284.8 eV. The occurrence of P 2p (132.6 eV for P(V) in Ag_3PO_4 [44]) and Ag 3d (374 eV and 368 eV for Ag $3d_{3/2}$ and Ag $3d_{5/2}$ [45], respectively, in Fig. S3 in ESI†) peaks in the XPS spectra of UAP-X verified that Ag_3PO_4 is undoubtedly interacted to the UiO-66-NH_2, which was also confirmed by both PXRD and FTIR analyses. In addition, the two peaks at 182.99 and 185.36 eV could be attributed to Zr-O clusters coordinated with the carboxylic groups of NH_2-BDC ligands in UiO-66-NH_2 [46–48]. The TGA results (Fig. 1d) demonstrate that the increase of UiO-66-NH_2 content in the UAP-X composites lead to the larger weight loss due to the loss of organic composition (NH_2-BDC ligands) from UiO-66-NH_2, and the residual weight of the final residue are also consistent with the different UiO-66-NH_2 content in the UAP-X samples.

The morphologies and micro-structures of Ag_3PO_4, UAP-X composites and UiO-66-NH_2 were investigated by both SEM and TEM (Figs. 2 and S4 in ESI†). As illustrated in Fig. 2, the SEM images revealed that the Ag_3PO_4 nanoparticles were clearly deposited on the surface of UiO-66-NH_2 and the average crystallite size of Ag_3PO_4 particles decreased with the increase of UiO-66-NH_2 content. The pure Ag_3PO_4 nanoparticles exhibited sphere-like structure with the particle sizes of range

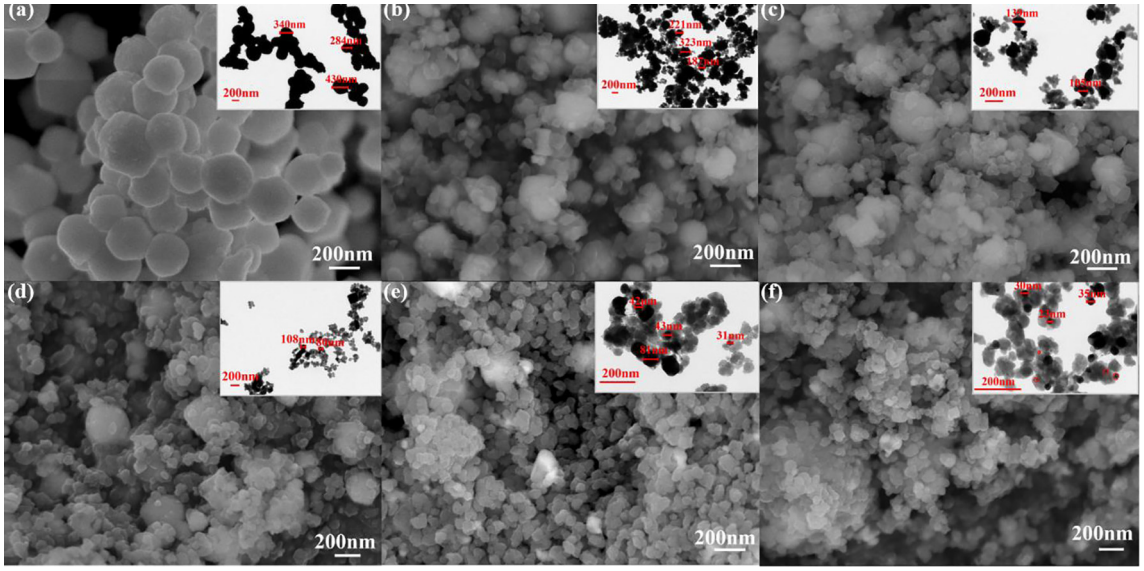

Fig. 2. SEM and TEM (inset) images of (a) Ag_3PO_4, (b) UAP-20, (c) UAP-35, (d) UAP-50, (e) UAP-120, (f) UAP-200.

from 250 to 450 nm as shown in the TEM image in Fig. 2a. Whereas, the crystallite size of Ag_3PO_4 particles UAP-200 is less than 40 nm (Fig. 2f). The standard N_2 adsorption measurements show the Brunauer-Emmett-Teller (BET) surface area decreased from 874.15 $m^2 g^{-1}$ (UiO-66-NH_2) to 424.4 $m^2 g^{-1}$ (UAP-200), 191.9 $m^2 g^{-1}$ (UAP-120), 103.5 $m^2 g^{-1}$ (UAP-50) and 67.2 $m^2 g^{-1}$ (UAP-35), which further confirm that the Ag_3PO_4 NPs were anchored with UiO-66-NH_2 (Table S1 in ESI†).

3.2. Adsorption and desorption performances of UAP-X toward SMX

3.2.1. The adsorption performances of Ag_3PO_4, UiO-66-NH_2 and UAP-X

Sulfamethoxazole (SMX) is known to possess two pK_a values (i.e. 1.7 and 5.7) [49], in which the major species of SMX were cationic (SMX^+) at pH < 1.7, neutral (SMX^0) at pH between 1.7 and 5.7, and anionic (SMX^-) at pH > 5.7 [50]. Under dark condition, Ag_3PO_4 particles can efficiently absorb SMX, in which nearly 100% SMX (initial concentration being 50 mg/L) can be adsorbed within 20 min, as shown in Fig. 3a. The uptake of SMX onto Ag_3PO_4 can be clearly observed in SEM images, as shown in Fig. 4(d) and (e). The zeta potentials of Ag_3PO_4 were measured in the pH ranging from 2.0 to 6.0 (Fig. S6 in ESI†), and the results revealed that the surface of Ag_3PO_4 was negative at pH > 3.13. In our study, the initial pH of the SMX aqueous solution (50 mg/L) was 4.52, which was similar to 4.38 reported by Zhang and coworker [51], indicating the adsorption toward SMX via weak electrostatic attraction cannot be negligible. While the –NH_2 group from SMX could be coordinated to Ag^+ in Ag_3PO_4 [52], which was affirmed by the XPS analysis. Specifically, the binding energy of N 1s in –NH_2 attached on SMX shifted from 399.79 eV in original SMX to 399.28 eV in SMX adsorbed onto Ag_3PO_4(Fig. 4b). The adsorption of SMX by Ag_3PO_4 led to a shift to higher energy for the Ag 3d from 368 eV ($3d_{5/2}$) and 374 eV ($3d_{3/2}$) in original Ag_3PO_4 to 368.37 eV and 374.37 eV in SMX@Ag_3PO_4 (Fig. 4c). The coordination interactions between –NH_2 and Ag^+ could also be affirmed by FTIR, in which the characteristic peak of –NH_2 at 1620 cm^{-1} for original SMX shifted to 1612 cm^{-1} for SMX@Ag_3PO_4 (Fig. S7 in ESI†) [52,53].

As illustrated in Fig. 3a, the individual UiO-66-NH_2 demonstrated poor SMX uptake (removal efficiency being 20%), which might result from the positive surface (the zeta potential being + 9.29 mV) of UiO-66-NH_2 and the neutral SMX. It is obvious that UAP-X (except for UAP-200) exhibited higher adsorption activities toward SMX compared with that of UiO-66-NH_2, in which the decrease of UiO-66-NH_2 content led to enhanced adsorption performance. As shown in Fig. 3a, nearly 100% SMX was adsorbed after 20 min dark adsorption for the Ag_3PO_4, UAP-20, and UAP-35, whereas UAP-200 captured about 60% SMX after 1 h dark adsorption.

As shown in Fig. 4a, the XPS spectra of Ag_3PO_4 and UAP-50 after the

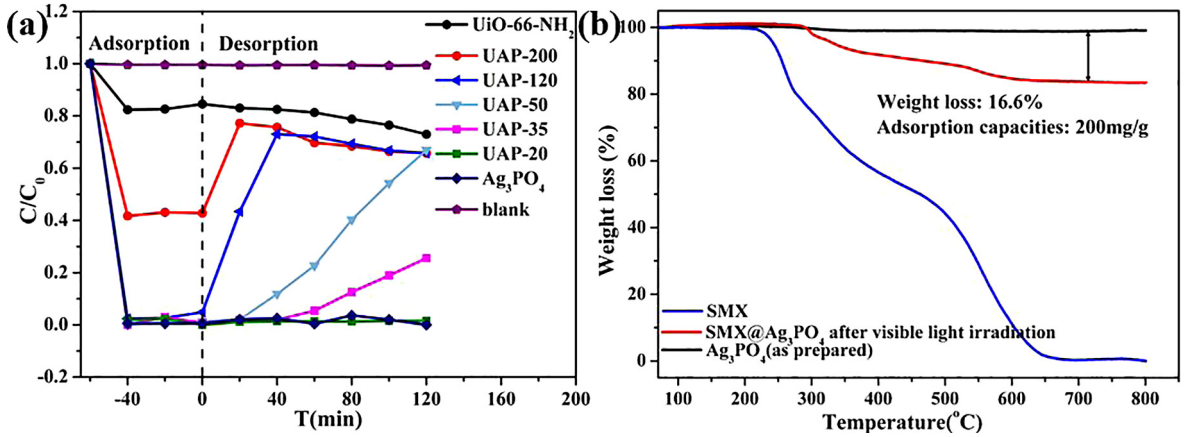

Fig. 3. (a) SMX adsorption and desorption performance of Ag_3PO_4, UAP-X (X = 20 mg, 35 mg, 50 mg, 120 mg and 200 mg) composites and UiO-66-NH_2. (b) TGA curves of as-prepared Ag_3PO_4, sulfamethoxazole (SMX) and Ag_3PO_4 treated after dark-adsorption SMX and visible light radiation for 2 h.

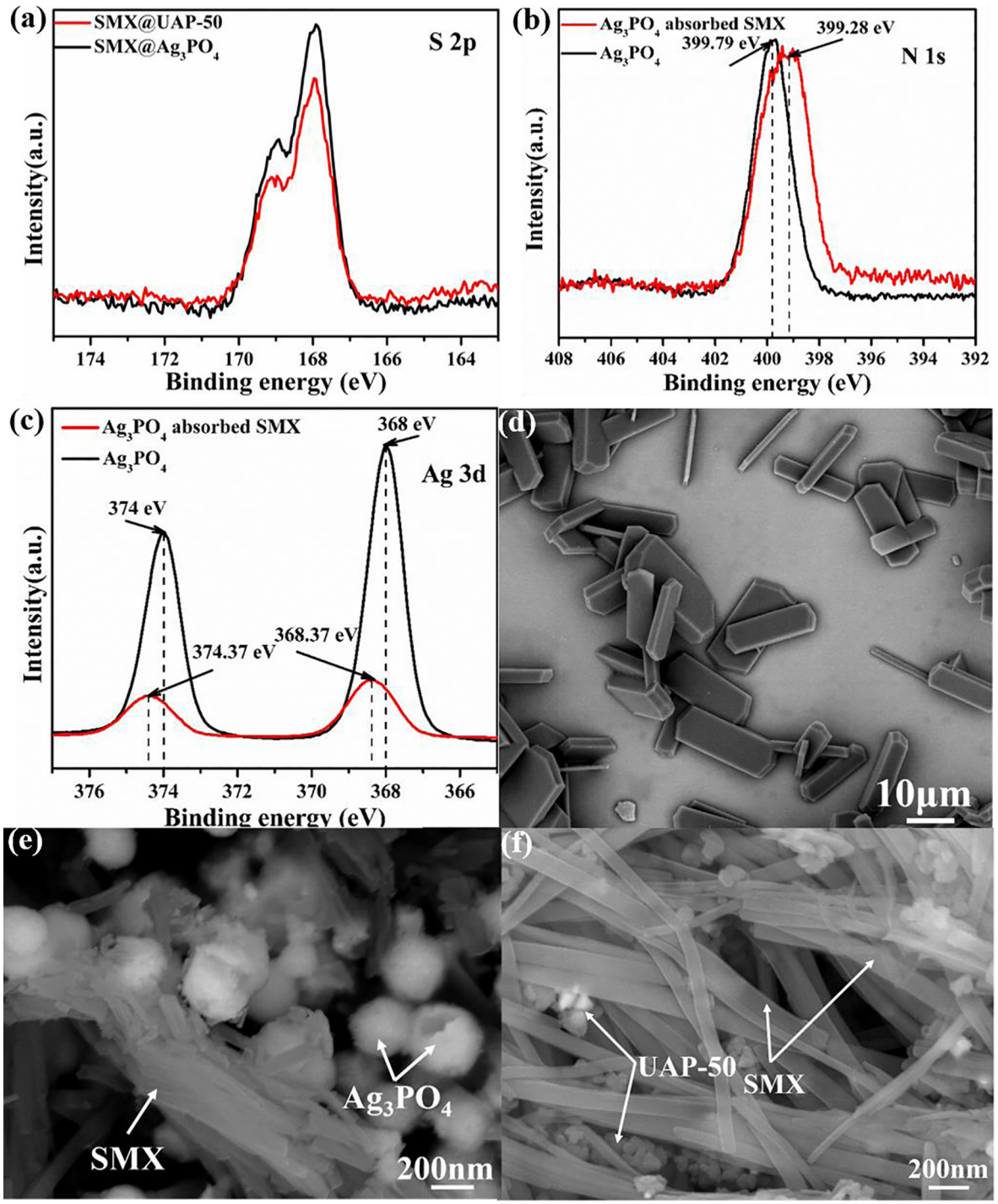

Fig. 4. (a) The XPS spectra for S2p in Ag_3PO_4 and UAP-50 after adsorbing SMX before visible light irradiation. (b) N 1s XPS spectra of SMX and Ag_3PO_4 after adsorbing SMX. (c) Ag 3d XPS spectra of Ag_3PO_4 before and after adsorbing SMX. (d) SEM image of SMX. (e, f) SEM images of Ag_3PO_4 and UAP-50 adsorbed SMX before the visible light irradiation.

adsorption of SMX revealed an S 2p peak originated from SMX, indicating the uptake of SMX via Ag_3PO_4 and UAP-50 composites. The SEM images (Fig. 4e and f) illustrated granule-like Ag_3PO_4, UiO-66-NH_2 and strip-like SMX, affirmed that SMX was adsorbed by Ag_3PO_4 and UAP-50, respectively. As illustrated in Fig. 3a, the introduction of small amount of UiO-66-NH_2 into Ag_3PO_4 (UAP-20) didn't influence its adsorption behaviors, as enough Ag_3PO_4 nanoparticles were exposed to adsorb SMX, while, large content UiO-66-NH_2 in UAP-X composites (such as in UAP-200) resulted into decrease of adsorption performance, due to possibly partial surface coverage by UiO-66-NH_2.

It has been reported that Ag_3PO_4 has high photocatalytic activity for the degradation organic pollutants under visible light irradiation. In the present work, the pure Ag_3PO_4 treated after dark-adsorption SMX and visible light radiation for 2 h, was characterized by TGA. Compared to as-prepared Ag_3PO_4, it can be observed that there was a new weight loss in the TGA curve of the treated Ag_3PO_4 (Fig. 3b), which matched well with the weight loss of SMX. Moreover, the experimental adsorption capacities (200 mg/g) of Ag_3PO_4 toward SMX were nearly equal to the calculated one, indicating there was no desorption and photocatalytic degradation of Ag_3PO_4 toward SMX.

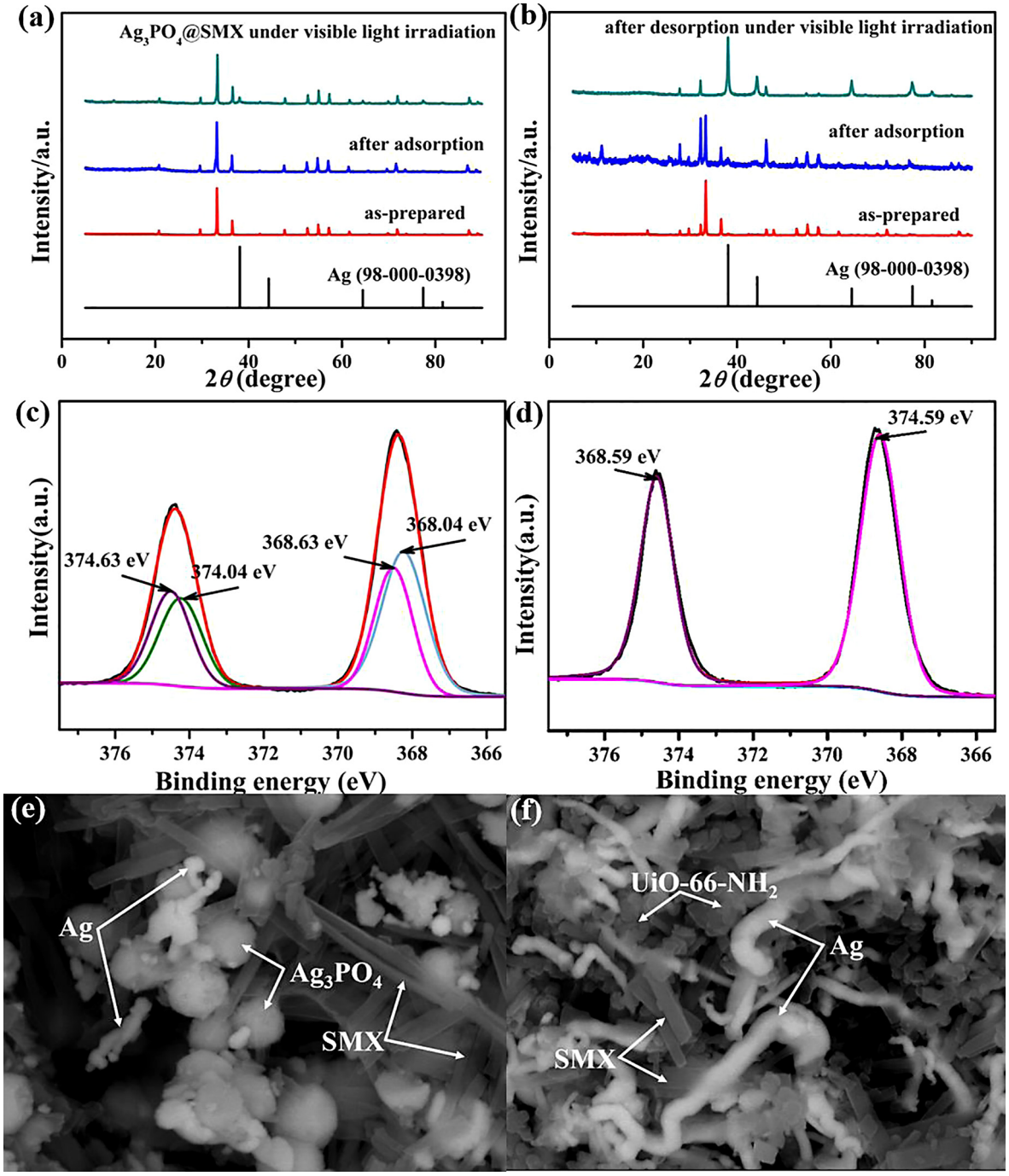

Fig. 5. (a, b) The PXRD patterns of Ag_3PO_4 and UAP-50 adsorbed SMX before and after the visible light irradiation. (c, d) Ag 3d XPS spectra of Ag_3PO_4 and UAP-50 adsorbed SMX after the visible light irradiation. (e, f) SEM images of Ag_3PO_4 and UAP-50 adsorbed SMX after the visible light irradiation.

3.2.2. The release of SMX from UAP-X under visible light

Light triggered desorption is pollution-free, nearly zero-energy cost and easy operation technique and has attracted increasing attentions. In this research, the series UAP-X (X ranging from 35 to 120) composites built from Ag_3PO_4 and UiO-66-NH_2 exhibited excellent desorption performance under the visible light irradiation, as shown in Fig. 3a. It is worthy to noting that individual Ag_3PO_4 possessed good adsorption of SMX in dark, while showed no desorption activity under visible light irradiation. Although the individual UiO-66-NH_2 exhibited poor adsorption and desorption behaviors, the introduction of UiO-66-NH_2 into Ag_3PO_4 (UAP-35, 50, 120) can induce the light-triggered desorption of SMX. Especially, the UAP-50/120 exhibited good desorption activities, in which ca. 66.9/73% SMX was released. As illustrated in Fig. 3a, the introduction of small amount of UiO-66-NH_2 into Ag_3PO_4 (UAP-20) didn't influence its adsorption and desorption behaviors, as its adsorption activity was mainly controlled by Ag_3PO_4 NPs. However, large content UiO-66-NH_2 was composited with Ag_3PO_4 (like UAP-200) resulted into decrease of adsorption performance and good desorption activity under the visible light irradiation.

It has been reported that the semiconductor Ag_3PO_4 particles can be photo-excited for water splitting under visible light irradiation ($\lambda < 530$ nm) [54,55]. During the photo-catalytically split of water molecules, the Ag^+ ions in Ag_3PO_4 NPs were simultaneously being reduced into Ag^0 following the Eq. (1) [29,56]. For UAP-35, 50 and 120 composites in our present work, visible light-induced transformation from Ag^+ to Ag^0 is believed as the possible mechanism for the SMX

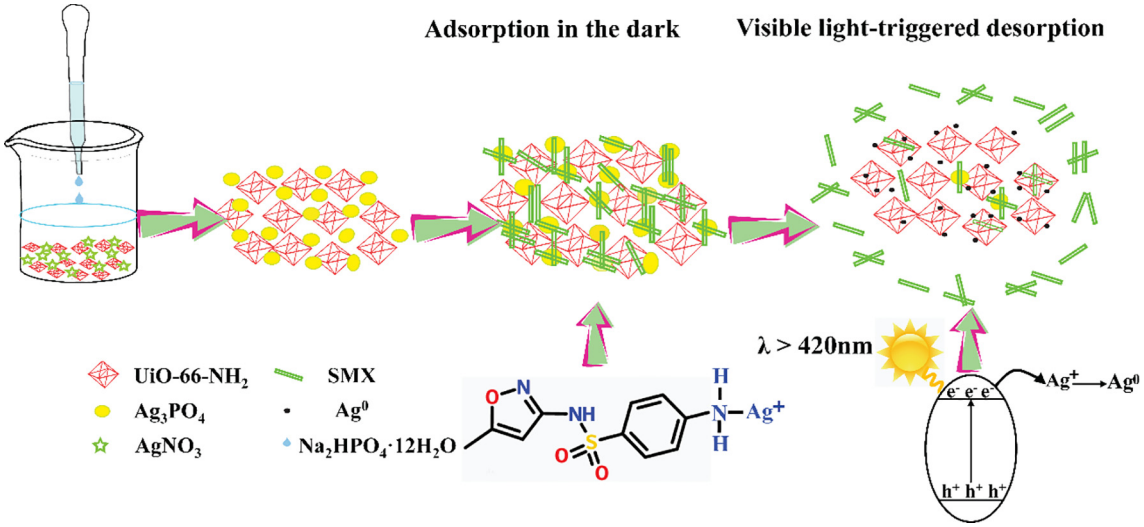

Fig. 6. The schematic diagram of the synthesis of UiO-66-NH_2/Ag_3PO_4 (UAP-X) MOF-NP composites and their adsorption-desorption mechanism.

release under visible light irradiation. The small size Ag_3PO_4 NPs facilitate the reduction of Ag^+, resulting in rapid decrease of adsorptive sites (Ag^+) and release of adsorbed SMX. Both SEM and TEM results illustrated in Fig. 2 revealed that smaller Ag_3PO_4 NPs can be made with increasing amount of UiO-66-NH_2 and the resulting Ag_3PO_4 NPs are dispersed on their surface of UiO-66-NH_2. Therefore, it is easy to understand why UAP-120 possessed good adsorption and desorption activities. As to UAP-200, the large content of UiO-66-NH_2 decreased its adsorption performance, while smaller Ag_3PO_4 NPs enhanced its desorption activity, as shown in Fig. 3a.

$$4Ag_3PO_4 + 6H_2\,O + 12h^+ + 12e^- \rightarrow 12Ag + 4H_3PO_4 + 3O_2 \quad (1)$$

For larger Ag_3PO_4 particles, the light irradiation could induce the Ag^+ reduction in limited extent due to its bigger particle size, which was affirmed by PXRD, XPS and SEM. As illustrated in Fig. 5a, the diffraction peaks at 29.70°, 33.29°, 36.59°, 55.02°, and 71.90° were the characteristics peaks of Ag_3PO_4 (JCPDS card No. 006-0505). And the diffraction peaks at 38.11°, 44.30°, 64.44°, 77.39° and 81.54° could be assigned to metallic silver (Ag^0) (JCPDS card No. 98-000-0398). After visible light irradiation for 2 h, the PXRD patterns of Ag_3PO_4 were nearly identical to both those of as-prepared Ag_3PO_4 and simulated ones, in which the characteristic peaks of Ag^0 were difficult to be detected due to the minor content. In Fig. 5b, the obvious presence of Ag^0 in UAP-50 could be evidenced by the occurrence of characteristic PXRD peaks of Ag^0. Furthermore, the main diffraction peak at $2\theta = 38.11°$ corresponding to Ag^0 of UiO-66-NH_2/Ag_3PO_4 composites, exhibited drastic enhanced peak intensity compared with that of Ag_3PO_4 after desorption and UiO-66-NH_2 has good light stability (Fig. S8 in ESI†). It can be seen from Fig. 5c that the XPS peaks of Ag 3d of individual Ag_3PO_4 NPs with adsorbed SMX under dark condition and Ag_3PO_4 NPs irradiated by visible light for 2 h could be further divided into four different peaks at 374.63, 374.04 eV and 368.63, 368.04 eV, respectively. The XPS peaks of Ag 3d of Ag_3PO_4 in UAP-50 with adsorbed SMX under dark condition and Ag_3PO_4 in UAP-50 being irradiated by visible light for 2 h were at 368.59 and 374.59 eV (Fig. 5d). According to the results reported by Zhang et al., the peaks at 374.6 and 368.6 eV could be attributed to Ag^0, whereas the peaks at 374.04 and 368.04 eV are attributed to Ag^+ ions in Ag_3PO_4 [57].

In this work, visible light-induced transform from Ag^+ to Ag^0 of Ag_3PO_4 was believed as possible mechanism for the release of SMX under visible light irradiation. The differences in efficiency of reduced Ag^0 between Ag_3PO_4 and UAP-50 are also shown in SEM images (Fig. 5e and f). There are only small amount of long strip-like Ag relatively and a large amount of Ag_3PO_4 with sphere-like structure for treated Ag_3PO_4 (Fig. 5e). Whereas, almost all are long strip-like Ag for treated UAP-50 (Fig. 5f). The presence of Ag species existed as metallic Ag was further confirmed. From three SEM images shown in Fig. S9 (in ESI†), long strip-like particles were not SMX molecules, UiO-66-NH_2 or Ag_3PO_4 particles, which were Ag° clusters. The difference of $Ag^+ - Ag^0$ reduction efficiency could be attributed to the Ag_3PO_4 nanoparticles aggregated quickly into micrometer-sized clusters in aqueous solutions and the particle size of Ag_3PO_4 shows an obvious effect on photo-oxidative reactions [58–60]. The large surface area of small-sized particles is expected to be beneficial for photocatalytic reactions that mostly occur on the surface of the catalysts. To clarify the detailed adsorption-desorption behavior of UAP-X composites toward SMX, the PXRD patterns of Ag_3PO_4 and UAP-50 adsorbing SMX under dark condition and being irradiated by visible light for 2 h were illustrated in Fig. 5a and b. Both Ag_3PO_4 and UAP-50 could keep stable after adsorbing SMX without light irradiation, and no Ag^0 peak was observed. SMX adsorbed by UAP-50 was released along with the reduction of Ag^+ to Ag^0 under the visible light irradiation. In addition, the PXRD patterns of Ag_3PO_4, UAP-50 and UAP-120 treated with dispersed in solvent without SMX and visible light irradiation for 2 h (Fig. S10 in ESI†) could affirm that the presence of SMX has no influence on the transformation from Ag^+ to Ag^0. The different composition ratio of UiO-66-NH_2 and Ag_3PO_4 has an obvious effect on the SMX release capacity. That can be attributed to that the smaller crystal size of Ag_3PO_4 particles with the increasing of UiO-66-NH_2 content in the composites. In addition, UiO-66-NH_2 could provide deposition area for Ag NPs to promote the release of SMX. Therefore, it was concluded that Ag^+ being reduced to Ag^0 under the visible light irradiation might be the possible mechanism leading to the release of SMX. To further confirm the SMX release from UAP-X, UPLC and Q-TOF-MS were utilized to conduct quantitative (concentration determination) and qualitative (SMX identification, as shown in Fig. S5 ESI†) analysis, the results revealed that SMX was actually released from UAP-50. The schematic diagram of synthesis method of UAP-X composites and adsorption-desorption mechanism were shown in Fig. 6.

4. Conclusion

In summary, UiO-66-NH_2/Ag_3PO_4 (UAP-X) MOF-nanoparticle composites were facilely prepared from aqueous solution by an in-situ ion-exchange precipitation method. By the combination the well-dispersed Ag_3PO_4 NPs on the UiO-66-NH_2 platform, the resulting composites can achieve good adsorption and desorption performance for SMX. For instance, UAP-50/120 possesses excellent adsorption (experimental adsorption capacity being 200 mg/g) and desorption (the

desorption amount being 134/146 mg/g) activities toward SMX. The visible light-triggered desorption of SMX on the UAP-X composite can be assigned to the transformation from Ag^+ in Ag_3PO_4 to Ag^0 under visible light irradiation and was found to be heavily dependent on the content of UiO-66-NH_2, resulting the first reported light-triggered desorption toward organic matters of MOF-NP composites, to our best knowledge. This work could open new opportunities for adsorption-desorption of targeted organic matters using visible light. Frankly, in this paper, the transformation from Ag^+ to Ag^0 under light irradiation was not reversible, which hindered the reutilization and potential application to remove environmental PPCPs pollutants. But, it leaves a window open for these composites to be used in drug delivery. Further researches are designed to facilely prepare similar MOFs-based composites to achieve their adsorption-desorption activities triggered by light toward targeted organic matters, which will knock a door open to achieve light induced desorption with zero-pollution and low-cost regeneration.

Acknowledgements

This work was supported by National Natural Science Foundation of China (51578034), Great Wall Scholars Training Program Project of Beijing Municipality Universities (CIT&TCD20180323), Project of Construction of Innovation Teams and Teacher Career Development for Universities and Colleges Under Beijing Municipality (IDHT20170508), Beijing Talent Project (2017A38), and the Fundamental Research Funds for Beijing Universities.

Appendix A. Supplementary data

Supplementary data associated with this article can be found, in the online version, at http://dx.doi.org/10.1016/j.cej.2018.06.005.

References

[1] D. Zhang, R.M. Gersberg, W.J. Ng, S.K. Tan, Removal of pharmaceuticals and personal care products in aquatic plant-based systems: a review, Environ. Pollut. 184 (2014) 620–639.
[2] Q. Bu, B. Wang, J. Huang, S. Deng, G. Yu, Pharmaceuticals and personal care products in the aquatic environment in China: a review, J. Hazard. Mater. 262 (2013) 189–211.
[3] S.-W. Nam, C. Jung, H. Li, M. Yu, J.R. Flora, L.K. Boateng, N. Her, K.-D. Zoh, Y. Yoon, Adsorption characteristics of diclofenac and sulfamethoxazole to graphene oxide in aqueous solution, Chemosphere 136 (2015) 20–26.
[4] J. Cao, R. Jiang, J. Wang, J. Sun, Q. Feng, Z. Zhao, G. Chen, C. Zhou, E. Yin, Study on the interaction mechanism between cefradine and *Chlamydomonas reinhardtii* in water solutions under dark condition, Ecotox. Environ. Safe. 159 (2018) 56–62.
[5] S. Thiele-Bruhn, Pharmaceutical antibiotic compounds in soils – a review, J. Plant Nutr. Soil Sci. 166 (2003) 145–167.
[6] I.Y. Hwang, E. Koh, H.R. Kim, W.S. Yew, M.W. Chang, Reprogrammable microbial cell-based therapeutics against antibiotic-resistant bacteria, Drug Resist. Update 27 (2016) 59–71.
[7] C.C. Wang, J.R. Li, X.L. Lv, Y.Q. Zhang, G. Guo, Photocatalytic organic pollutants degradation in metal–organic frameworks, Energy Environ. Sci. 7 (2014) 2831–2867.
[8] H.-R. Buser, T. Poiger, M.D. Müller, Occurrence and fate of the pharmaceutical drug diclofenac in surface waters: rapid photodegradation in a lake, Environ. Sci. Technol. 32 (1998) 3449–3456.
[9] G.R. Boyd, H. Reemtsma, D.A. Grimm, S. Mitra, Pharmaceuticals and personal care products (PPCPs) in surface and treated waters of Louisiana, USA and Ontario, Canada, Sci. Total Environ. 311 (2003) 135–149.
[10] A. Joss, S. Zabczynski, A. Göbel, B. Hoffmann, D. Löffler, C.S. McArdell, T.A. Ternes, A. Thomsen, H. Siegrist, Biological degradation of pharmaceuticals in municipal wastewater treatment: proposing a classification scheme, Water Res. 40 (2006) 1686–1696.
[11] G.R. Boyd, S. Zhang, D.A. Grimm, Naproxen removal from water by chlorination and biofilm processes, Water Res. 39 (2005) 668–676.
[12] S. Esplugas, D.M. Bila, L.G.T. Krause, M. Dezotti, Ozonation and advanced oxidation technologies to remove endocrine disrupting chemicals (EDCs) and pharmaceuticals and personal care products (PPCPs) in water effluents, J. Hazard. Mater. 149 (2007) 631–642.
[13] M. Klavarioti, D. Mantzavinos, D. Kassinos, Removal of residual pharmaceuticals from aqueous systems by advanced oxidation processes, Environ. Int. 35 (2009) 402–417.
[14] X.D. Du, C.C. Wang, J.G. Liu, X.D. Zhao, J. Zhong, Y.X. Li, J. Li, P. Wang, Extensive and selective adsorption of ZIF-67 towards organic dyes: performance and mechanism, J. Colloid Interface Sci. 506 (2017) 437–441.
[15] X. Zhao, Y. Wei, H. Zhao, Z. Gao, Y. Zhang, L. Zhi, Y. Wang, H. Huang, Functionalized metal-organic frameworks for effective removal of rocephin in aqueous solutions, J. Colloid Interface Sci. 514 (2017) 234–239.
[16] J.J. Li, C.C. Wang, H.F. Fu, J.R. Cui, P. Xu, J. Guo, J.R. Li, High-performance adsorption and separation of anionic dyes in water using a chemically stable graphene-like metal-organic framework, Dalton Trans. 46 (2017) 10197–10201.
[17] D. Sheng, L. Zhu, C. Xu, C. Xiao, Y. Wang, Y. Wang, L. Chen, J. Diwu, J. Chen, Z. Chai, T.E. Albrecht-Schmitt, S. Wang, Efficient and selective uptake of TcO_4^- by a cationic metal-organic framework material with open Ag^+ sites, Environ. Sci. Technol. 51 (2017) 3471–3479.
[18] W. He, N. Li, X. Wang, T. Hu, X. Bu, A cationic metal-organic framework based on Zn4 cluster for rapid and selective adsorption of dyes, Chin. Chem. Lett. 4276 (2017).
[19] L. Zhu, D. Sheng, C. Xu, X. Dai, M.A. Silver, J. Li, P. Li, Y. Wang, Y. Wang, L. Chen, C. Xiao, J. Chen, R. Zhou, C. Zhang, O.K. Farha, Z. Chai, T.E. Albrecht-Schmitt, S. Wang, Identifying the recognition site for selective trapping of $^{99}TcO_4$- in a hydrolytically stable and radiation resistant cationic metal-organic framework, J. Am. Chem. Soc. 139 (2017) 14873–14876.
[20] Y. Peng, Y. Zhang, H. Huang, C. Zhong, Flexibility induced high-performance MOF-based adsorbent for nitroimidazole antibiotics capture, Chem. Eng. J. 333 (2018) 678–685.
[21] X. Zhao, H. Zhao, W. Dai, Y. Wei, Y. Wang, Y. Zhang, L. Zhi, H. Huang, Z. Gao, A metal-organic framework with large 1-D channels and rich OH sites for high-efficiency chloramphenicol removal from water, J. Colloid Interface Sci. 526 (2018) 28–34.
[22] Y. Li, Z. Yang, Y. Wang, Z. Bai, T. Zheng, X. Dai, S. Liu, D. Gui, W. Liu, M. Chen, L. Chen, J. Diwu, L. Zhu, R. Zhou, Z. Chai, T.E. Albrecht-Schmitt, S. Wang, A mesoporous cationic thorium-organic framework that rapidly traps anionic persistent organic pollutants, Nat. Commun. 8 (2017) 1354.
[23] M. Nazari, M. Rubio-Martinez, G. Tobias, J.P. Barrio, R. Babarao, F. Nazari, K. Konstas, B.W. Muir, S.F. Collins, A.J. Hill, Metal-organic-framework-coated optical fibers as light-triggered drug delivery vehicles, Adv. Funct Mater. 26 (2016) 3244–3249.
[24] T. Zheng, Z. Yang, D. Gui, Z. Liu, X. Wang, X. Dai, S. Liu, L. Zhang, Y. Gao, L. Chen, D. Sheng, Y. Wang, J. Diwu, J. Wang, R. Zhou, Z. Chai, T.E. Albrecht-Schmitt, S. Wang, Overcoming the crystallization and designability issues in the ultrastable zirconium phosphonate framework system, Nat. Commun. 8 (2017) 15369.
[25] J. Park, D. Yuan, K.T. Pham, J.-R. Li, A. Yakovenko, H.-C. Zhou, Reversible alteration of CO_2 adsorption upon photochemical or thermal treatment in a metal-organic framework, J. Am. Chem. Soc. 134 (2011) 99–102.
[26] W. Zheng, G.F. Strouse, Involvement of carriers in the size-dependent magnetic exchange for Mn:CdSe quantum dots, J. Am. Chem. Soc. 133 (2011) 7482–7489.
[27] W. Zheng, Y. Liu, A. West, E.E. Schuler, K. Yehl, R.B. Dyer, J.T. Kindt, K. Salaita, Quantum dots encapsulated within phospholipid membranes: phase-dependent structure, photostability, and site-selective functionalization, J. Am. Chem. Soc. 136 (2014) 1992–1999.
[28] J. Aguilera-Sigalat, D. Bradshaw, Synthesis and applications of metal-organic framework-quantum dot (QD@MOF) composites, Coord. Chem. Rev. 307 (2016) 267–291.
[29] Z. Yi, J. Ye, N. Kikugawa, T. Kako, S. Ouyang, H. Stuart-Williams, H. Yang, J. Cao, W. Luo, Z. Li, An orthophosphate semiconductor with photooxidation properties under visible-light irradiation, Nat. Mater. 9 (2010) 559–564.
[30] L. Luo, Y. Li, J. Hou, Y. Yang, Visible photocatalysis and photostability of Ag_3PO_4 photocatalyst, Appl. Surf. Sci. 319 (2014) 332–338.
[31] J.-M. Schumers, C.-A. Fustin, J.-F. Gohy, Light-responsive block copolymers, Macromol. Rapid Commu. 31 (2010) 1588–1607.
[32] Y. Wei, S. Han, J. Kim, S. Soh, B.A. Grzybowski, Photoswitchable catalysis mediated by dynamic aggregation of nanoparticles, J. Am. Chem. Soc. 132 (2010) 11018–11020.
[33] Y. Shiraishi, K. Tanaka, E. Shirakawa, Y. Sugano, S. Ichikawa, S. Tanaka, T. Hirai, Light-triggered self-assembly of gold nanoparticles based on photoisomerization of spirothiopyran, Angew. Chem. Int. Edit. 52 (2013) 8304–8308.
[34] M. Kandiah, M.H. Nilsen, S. Usseglio, S. Jakobsen, U. Olsbye, M. Tilset, C. Larabi, E.A. Quadrelli, F. Bonino, K.P. Lillerud, Synthesis and Stability of Tagged UiO-66 Zr-MOFs, Chem. Mater. 22 (2010) 6632–6640.
[35] C. Cui, Y. Wang, D. Liang, W. Cui, H. Hu, B. Lu, S. Xu, X. Li, C. Wang, Y. Yang, Photo-assisted synthesis of Ag_3PO_4 /reduced graphene oxide/Ag heterostructure photocatalyst with enhanced photocatalytic activity and stability under visible light, Appl. Catal. B: Environ. 158–159 (2014) 150–160.
[36] F.A. Sofi, K. Majid, Enhancement of the photocatalytic performance and thermal stability of an iron based metal-organic-framework functionalised by Ag/Ag_3PO_4, Mater. Chem. Front. (2018), http://dx.doi.org/10.1039/C8QM00051D.
[37] L. Shen, S. Liang, W. Wu, R. Liang, L. Wu, Multifunctional NH_2-mediated zirconium metal-organic framework as an efficient visible-light-driven photocatalyst for selective oxidation of alcohols and reduction of aqueous Cr(VI), Dalton Trans. 42 (2013) 13649–13657.
[38] D. Sun, Y. Fu, W. Liu, L. Ye, D. Wang, L. Yang, X.Z. Fu, Z.H. Li, Studies on photocatalytic CO_2 reduction over NH_2-Uio-66(Zr) and its derivatives: towards a better understanding of photocatalysis on metal-organic frameworks, Chem. Eur. J. 19 (2013) 14279–14285.
[39] P. Kanoo, K.L. Gurunatha, T.K. Maji, Versatile functionalities in MOFs assembled from the same building units: interplay of structural flexibilty, rigidity and regularity, J. Mater. Chem. 20 (2010) 1322–1331.
[40] J. Yang, Y. Dai, X. Zhu, Z. Wang, Y. Li, Q. Zhuang, J. Shi, J. Gu, Metal–organic

frameworks with inherent recognition sites for selective phosphate sensing through their coordination-induced fluorescence enhancement effect, J. Mater. Chem. A 3 (2015) 7445–7452.
[41] X. Cheng, A. Zhang, K. Hou, M. Liu, Y. Wang, C. Song, G. Zhang, X. Guo, Size- and morphology-controlled NH_2-MIL-53(Al) prepared in DMF-water mixed solvents, Dalton Trans. 42 (2013) 13698–13705.
[42] L. Valenzano, B. Civalleri, S. Chavan, S. Bordiga, M.H. Nilsen, S. Jakobsen, K.P. Lillerud, C. Lamberti, Disclosing the complex structure of UiO-66 metal organic framework: a synergic combination of experiment and theory, Chem. Mater. 23 (2011) 1700–1718.
[43] M. Thomas, S. Ghosh, K. George, Characterisation of nanostructured silver orthophosphate, Mater. Lett. 56 (2002) 386–392.
[44] P. Ma, H. Yu, Y. Yu, W. Wang, H. Wang, J. Zhang, Z. Fu, Assembly of Ag_3PO_4 nanoparticles on two-dimensional Ag_2S sheets as visible-light-driven photocatalysts, Phys. Chem. Chem. Phys. 18 (2016) 3638–3643.
[45] H. Zhang, G. Wang, D. Chen, X. Lv, J. Li, Tuning photoelectrochemical performances of Ag-TiO_2 nanocomposites via reduction/oxidation of Ag, Chem. Mater. 20 (2008) 6543–6549.
[46] J. Long, S. Wang, Z. Ding, S. Wang, Y. Zhou, L. Huang, X. Wang, Amine-functionalized zirconium metal-organic framework as efficient visible-light photocatalyst for aerobic organic transformations, Chem. Commun. 48 (2012) 11656–11658.
[47] Q. Wu, D. Wu, Y. Guan, Hybrid titania–zirconia nanoparticles coated adsorbent for highly selective capture of nucleosides from human urine in physiological condition, Anal. Chem. 86 (2014) 10122–10130.
[48] R. Wang, L. Gu, J.J. Zhou, X.L. Liu, F. Tong, C.H. Li, Y.H. Shen, Y.P. Yuan, Quasi-polymeric metal-organic framework UiO-66/g-C_3N_4 heterojunctions for enhanced photocatalytic hydrogen evolution under visible light irradiation, Adv. Mater. Interfaces 2 (2015) 1500037.
[49] H. Lucida, J.E. Parkin, V.B. Sunderland, Kinetic study of the reaction of sulfamethoxazole and glucose under acidic conditions: I. Effect of pH and temperature, Int. J. Pharmaceut. 202 (2000) 47–62.
[50] D. Zhang, B. Pan, M. Wu, B. Wang, H. Zhang, H. Peng, D. Wu, P. Ning, Adsorption of sulfamethoxazole on functionalized carbon nanotubes as affected by cations and anions, Environ. Pollut. 159 (2011) 2616–2621.
[51] D. Zhang, B. Pan, H. Zhang, P. Ning, B. Xing, Contribution of different sulfamethoxazole species to their overall adsorption on functionalized carbon nanotubes, Environ. Sci. Technol. 44 (2010) 3806–3811.
[52] L. Zhang, S. Yang, T. Han, L. Zhong, C. Ma, Improvement of Ag(I) adsorption onto chitosan/triethanolamine composite sorbent by an ion-imprinted technology, Appl. Surf. Sci. 263 (2012) 696–703.
[53] A. Liu, C.-C. Wang, C.-Z. Wang, H.-F. Fu, W. Peng, Y.-L. Cao, H.-Y. Chu, A.-F. Du, Selective adsorption activities toward organic dyes and antibacterial performance of silver-based coordination polymers, J. Colloid Interface Sci. 512 (2018) 730–739.
[54] X. Yang, H. Cui, Y. Li, J. Qin, R. Zhang, H. Tang, Fabrication of Ag_3PO_4-graphene composites with highly efficient and stable visible light photocatalytic performance, ACS Catal. 3 (2013) 363–369.
[55] T. Wei, X. Li, Q. Zhao, J. Zhao, D. Zhang, In situ capture of active species and oxidation mechanism of RhB and MB dyes over sunlight-driven Ag/Ag_3PO_4 plasmonic nanocatalyst, Appl. Catal. B: Environ. 125 (2012) 538–545.
[56] Y. Bi, S. Ouyang, N. Umezawa, J. Cao, J. Ye, Facet effect of single-crystalline Ag_3PO_4 sub-microcrystals on photocatalytic properties, J. Am. Chem. Soc. 133 (2011) 6490–6492.
[57] H. Zhang, G. Wang, D. Chen, X. Lv, J. Li, Tuning photoelectrochemical performances of Ag−TiO_2 nanocomposites via reduction/oxidation of Ag, Chem. Mater. 20 (2008) 6543–6549.
[58] P.V. Kamat, Photochemistry on nonreactive and reactive (semiconductor) surfaces, Chem. Rev. 93 (1993) 267–300.
[59] C.T. Dinh, T.D. Nguyen, F. Kleitz, Large-scale synthesis of uniform silver orthophosphate colloidal nanocrystals exhibiting high visible light photocatalytic activity, Cheminform 47 (2011) 7797–7799.
[60] J. Ma, J. Zou, L. Li, C. Yao, T. Zhang, D. Li, Synthesis and characterization of Ag_3PO_4 immobilized in bentonite for the sunlight-driven degradation of Orange II, Appl. Catal. B: Environ. 134 (2013) 1–6.